Microscopic Mechanism of Chiral Induction in a Metal−Organic Framework

Jack D. Evans and François-Xavier Coudert*

Chimie ParisTech, PSL Research University, CNRS, Institut de Recherche de Chimie Paris, 75005 Paris, France

S *Supporting Information*

ABSTRACT: The recently reported process of chiral induction in a metal−organic framework (MOF) by nonchiral guest adsorption, demonstrated on the prototypical MOF-5, may revolutionize the production of MOFs for enantioselective separation and catalysis. Herein, we describe an investigation employing multiscale molecular simulation to discover the microscopic mechanism of chiral induction and investigate the stability of the resulting framework. Our results explain how the molecular size and chemical nature of *N*-methyl-2-pyrrolidone (NMP) give rise to the chiral transformation in MOF-5, whereas it cannot occur for other guest molecules, such as *N,N*-dimethylformamide (DMF). Moreover, we show that the guest-free CMOF-5 structure is energetically unstable, with either the achiral conventional structure or a closed pore structure preferred, demonstrating that chirality will not be retained upon activation of CMOF-5. While this limits the usability of chiral induction in MOFs, our study opens new avenues for the use of other guest molecules and provides microscopic insight into this unexpected outcome of guest−framework interactions in a soft porous crystal.

Metal−organic frameworks (MOFs) are a class of nanoporous materials constructed in a modular approach by the combination of inorganic nodes and organic links.[1] There is fervent research in the production of chiral MOF materials for particular applications in enantioselective separation and catalysis.[2,3] Traditionally, chiral MOFs are produced by using chiral starting materials[4] or as a result of specific framework topologies.[5] Often, however, these materials are observed as racemic conglomerates.[6]

Recently, Zaworotko and co-workers[7] reported the exciting preparation of a chiral polymorph of the prototypical metal−organic framework MOF-5 (also known as IRMOF-1).[8] This was achieved by conducting conventional solvothermal synthesis in the presence of enantiopure proline or, alternatively, postsynthetic modification by immersion in *N*-methyl-2-pyrrolidone (NMP), an achiral solvent. The framework CMOF-5 crystallizes in the cubic chiral space group $P2_13$ and appears as a distorted structure of the familiar MOF-5, as demonstrated in Figure 1. This report of CMOF-5 suggested that the production and stability of a chirally induced MOF is strongly correlated to the adsorption of guest molecules: although induction of chirality by chiral guest adsorption has been reported before,[9,10] its occurrence upon adsorption of achiral molecules is novel and
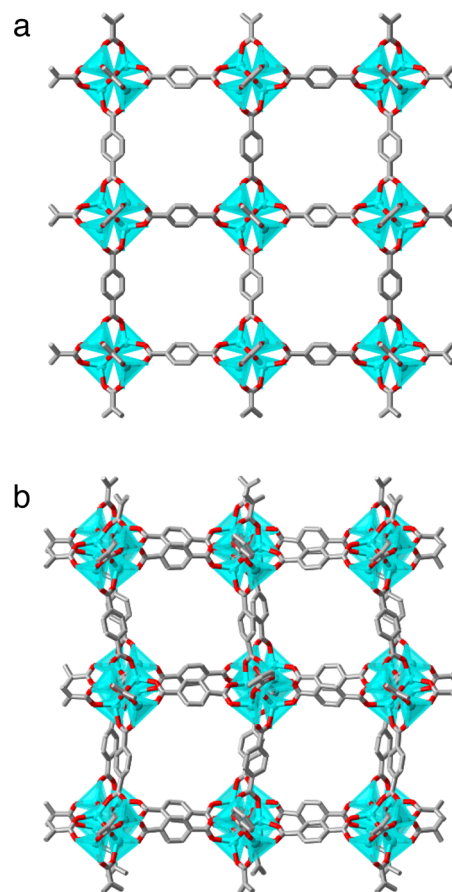

Figure 1. Structures of (a) achiral MOF-5 and (b) the Δ enantiomer of chiral MOF-5 (CMOF-5). Hydrogen atoms have been omitted for clarity. (Zn_4O, blue; O, red; C, gray).

entirely unexpected. NMP was observed to be crucial for chiral formation; upon subsequent solvent exchange with a variety of organic solvents a crystal-to-crystal transformation to achiral MOF-5 occurs. It is unclear so far how the action of NMP leads to chiral induction and whether an activated sample of CMOF-5 retains a chiral structure after NMP evacuation.

In this investigation, we examine the intrinsic stability of CMOF-5 using quantum chemistry calculations at the density functional theory (DFT) level, which have been thoroughly used to probe the mechanical stability of crystalline materials.[11,12]

DFT simulations suggest that chiral induction produces a metastable guest-loaded state, which is unlikely to be stable upon guest removal. Furthermore, by combining DFT calculations with Monte Carlo (MC) simulations we probe the mechanism for this guest-induced polymorphism.

We began this study by looking at the behavior of the chiral CMOF-5 structure in the absence of guest molecules. Starting from the Δ-CMOF-5 and Λ-CMOF-5 crystal structures, we removed the NMP solvent molecules and produced an ordered model. We then performed DFT energy minimization, optimizing both atomic coordinates and unit cell parameters. Calculations were performed using the CRYSTAL14 software[13,14] with localized TZVP basis sets and the solid-adapted hybrid exchange−correlation functional PBESOL0[15,16] (see Supporting Information for full details and input files). We observe that although some differences are present in the crystallographic structures, the Δ and Λ enantiomers of CMOF-5 behave identically. Upon energy minimization, in the absence of NMP, both structures relax back to the achiral MOF-5 structure. This indicates that CMOF-5 is not stable upon guest evacuation but spontaneously reverts back to the parent MOF-5 framework. We measure the energy difference between the two to be 9.33−11.1 kJ/mol per Zn_4O unit. This is likely to severely limit the use of chiral CMOF-5 to applications that do not require evacuation of the framework.

In an effort to capture the role of guests in chiral induction, we then placed 24 molecules of *N*-methyl-2-pyrrolidone (NMP) and *N,N*-dimethylformamide (DMF) in the Δ-CMOF-5 unit cell. Guests were positioned in the asymmetric unit to create an ordered structure that retains the $P2_13$ symmetry of CMOF-5 while avoiding atom−atom overlap. Optimization of both lattice parameters and atomic positions resulted in the converged structures illustrated in Figure 2, with sharp contrast between the two guests. Like evacuated CMOF-5, the structure loaded with DMF relaxes to an achiral MOF-5 structure, Figure 2a,b, with cell parameters and geometry similar to guest-free MOF-5 (no twisting of the linker). Conversely, the structure with NMP retained the chirality and geometric characteristics attributed to CMOF-5, Figure 2c,d; namely, a twist in the phenyl plane dihedral angle and adjacent Zn_4O cluster angle, in good agreement to the reported crystal structure.

The contrasting interaction of DMF and NMP with the framework can be qualitatively understood by observation of the local clustering of guests in the converged structure, Figure 2b,d. DMF is found in close distances to the Zn_4O cluster, and with a strong adsorption enthalpy of 98.1 kJ/mol (see Table 1). This is in agreement with a recent study, which reports this strong binding is key to the formation of cobalt substituted MOF-5 analogues.[17] NMP, in contrast to DMF, is observed to converge closer to the phenyl ligand since it is unable to achieve close contact to the Zn_4O cluster because of its size of NMP. Furthermore, NMP is found in close contact (∼4 Å) to adjacent NMP molecules, with guest−guest interactions stronger than DMF. This NMP-mediated "bridging" of neighboring aromatic rings creates the internal shearing stress that induces chirality in CMOF-5 by twisting the linkers. Notably, the interaction between NMP and the framework is dispersive in nature. Additionally, we find this "bridging" mechanism to be loading dependent revealed by further optimizations, with 12 NMP molecules per unit cell, converged to give the achiral MOF-5 structure.

While the DFT simulations detailed above give insight into NMP and DMF adsorption in MOF-5, and the reasons behind
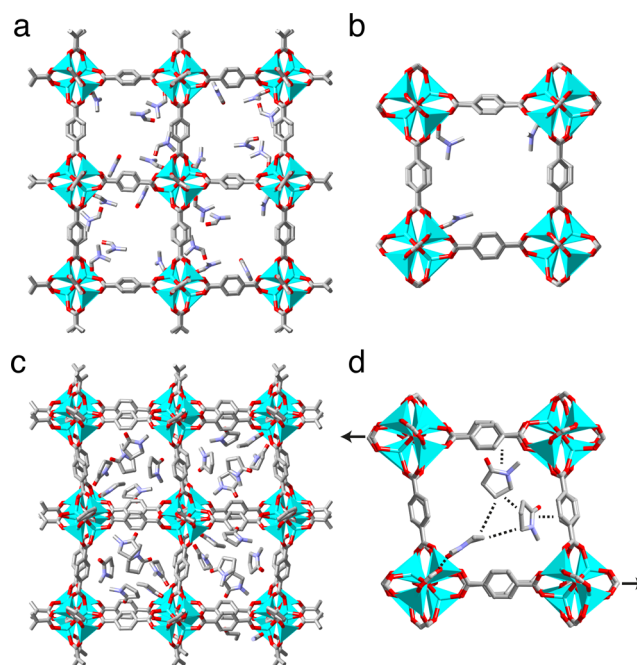

Figure 2. Local minima identified by DFT optimizations for DMF (a,b) and NMP (c,d) loaded structures of CMOF-5. $2 \times 2 \times 2$ unit cells (a,c) illustrate the extent of chiral induction, and a closer view (b,d) depicts the distinct local ordering of guest molecules. Additionally, close contacts (d, dotted lines) are depicted and the change in framework, simplified in two-dimensions. Hydrogen atoms have been omitted for clarity.

Table 1. Interaction Energies of DMF and NMP in CMOF-5 As Calculated from DFT Optimizations with Grimme's DFT-D2 Correction,[18] in Units kJ/mol Per Guest Molecule; Energies Are Calculated for Both Guest−MOF and Guest−Guest Interactions

	$\Delta E_{guest-MOF}$	$\Delta E_{guest-guest}$
$24 \times$ DMF	−98.1	−10.1
$12 \times$ DMF	−173	7.56
$24 \times$ NMP	−48.9	−18.5
$12 \times$ NMP	−136	−15.7

NMP inducing chirality, they form by their nature a static picture. To obtain a thermodynamic description of guest adsorption at a higher scale we employed classical Monte Carlo (MC) simulation in the *NVT* ensemble to describe DMF and NMP adsorption. We employed the RASPA classical simulation package,[19] and a detailed description of the methodology can be found in the Supporting Information.

In good agreement with the DFT simulations, MC simulations show that DMF and NMP adsorb in different sites in the framework's pore space. The distribution density of the guests averaged over the MC simulation is displayed in Figure 3. DMF adsorbs to the Zn_4O clusters with a second site at the center of the cage, in a similar appearance to that described of benzene.[20,21] As with the configuration observed by DFT optimization, we find NMP adjacent to the ligands and in well-defined positions. Unlike DMF, the cloud of density probability for NMP shows the guest-mediated benzene−benzene bridging that is responsible at the microscopic level for chiral induction. This visualization is confirmed by calculation of radial distribution functions (RDFs) between the framework and oxygen atom of the guest, plotted in
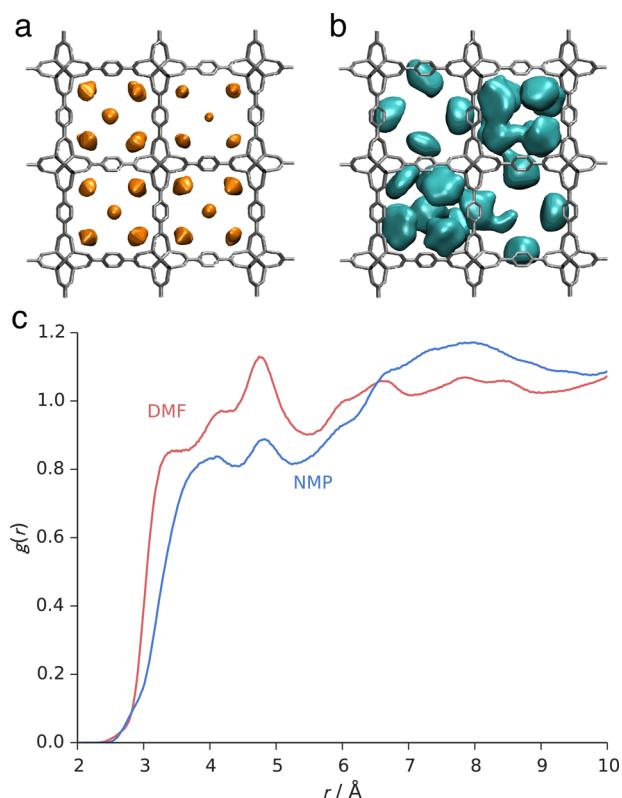
Figure 3. Average density distributions of DMF and NMP in MOF-5 at 298 K (a,b). The surface is shown here for a density value of 0.5 Å^{-3}. In addition, radial distribution functions (c) of DMF and NMP oxygen atoms and the framework present the different interactions observed.

Figure 4. Energy landscape with respect to cell volume, computed by DFT simulation, for different symmetries of MOF-5. Moreover, the relative volume of CMOF-5 reported by single crystal X-ray crystallography (dotted vertical line) and third-order Birch–Murnaghan equations of state are depicted (solid lines).

Figure 3c. This shows that average distances between NMP and the metal cluster is ~1 Å larger than for DMF.

This detailed picture of guest adsorption, obtained by multiscale molecular simulation, shows that it is the specific position of adsorbed NMP guests that is crucial to the formation of CMOF-5. Unsurprisingly, we find DFT optimizations of guest-free CMOF-5 to converge to give the achiral structure of MOF-5. To explore the energy landscape of guest-free CMOF-5 we conducted constrained cell DFT optimizations, beginning from the CMOF-5 structure, and compared these to the symmetry of conventional MOF-5, as plotted in Figure 4.

The energy landscape of $P2_13$ (CMOF-5) crystal symmetry is in stark contrast to that of the achiral $Fm\bar{3}m$ (MOF-5). Upon fitting third-order Birch–Murnaghan equations of state to the resulting energies[22] (see Supporting Information for full details) we find the $Fm\bar{3}m$ crystal symmetry gives a bulk modulus of 13.5 GPa, equivalent to that reported for MOF-5 by alternative methods.[11,23] However, the $P2_13$ structure is softer with non-Birch–Murnaghan behavior as identified by the poor fit and negative B_0', the first derivative of bulk modulus with respect to changes of volume. A number of materials, including ZIF-8[24] and MIL-53(Cr),[25] show similar behavior, attributed to structural transitions with the application of hydrostatic pressure. Examining $P2_13$ framework structures at large deformations by DFT optimizations we discovered a local minimum energy structure corresponding to a previously unrealized closed pore analogue of MOF-5. This structure has −51.6% cell volume, compared to the conventional MOF-5 structure, and is found to exhibit no geometrically accessible surface area or pore volume. Though thi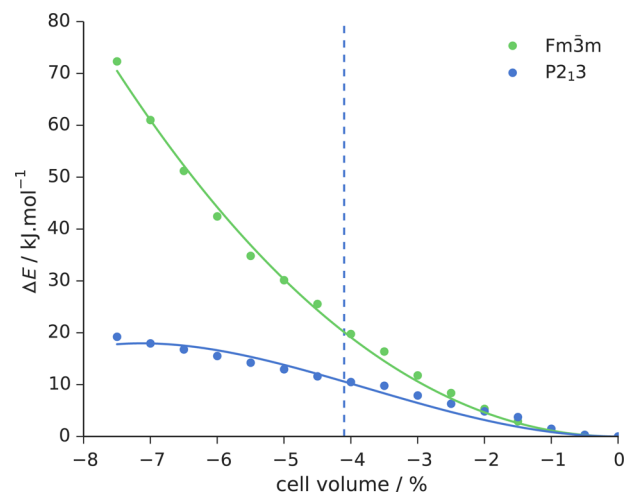s previously undiscovered structure is stable, the transition requires NMP adsorption, the application of hydrostatic pressure and subsequent NMP desorption. Notwithstanding, similar features of this transition have been observed for MOF-5 during water adsorption and negative thermal expansion.[26,27]

Resulting from the simulations presented here, the mechanism for chiral induction in MOF-5 requires a very specific deformation of cell volume. In the case for CMOF-5, this is achieved by the occluded NMP guest, which owing to its size can not adsorb closely to Zn_4O cluster. Notably, there is precedence for guest-induced volume shrinkage in MOFs.[28,29] However, NMP adsorption is a unique case where the framework deformation results in a chiral structure accomplished by more favorable torsional and angle deformation to the Zn_4O cluster than compression of bond lengths. It is the specific adsorption pattern of NMP, creating symmetry-lowering shear stress by bridging neighboring aromatic rings in the organic linker.

In summary, we have explored the recently reported chiral induction of MOF-5 by a multiscale molecular simulation approach. Though it may have been foreseeable to be general in nature, this effect is discovered to result from very specific interactions between NMP and MOF-5. Furthermore, DFT simulations have illustrated the instability of a guest-free CMOF-5 framework and the discovery of a closed pore analogue of MOF-5. To produce a stable guest-free framework by chiral induction, for applications including gas adsorption, an additional modification step is required to stabilize (or tie) the structure in the unstable chiral form. Similar methods have been recently exploited to stabilize a flexible porous organic cage.[30] Nonetheless, the details of chiral induction uncovered here give excellent insight for future experimental studies to discover new examples of this approach to chiral MOF synthesis.

■ ASSOCIATED CONTENT

Ⓢ Supporting Information

The Supporting Information is available free of charge on the ACS Publications website at DOI: 10.1021/jacs.6b02781.

Details of computational methods, comparison of chiral enantiomers, tabulated structural features, interaction

energies, Birch−Murnaghan coefficients, and additional figures (PDF)

AUTHOR INFORMATION

Corresponding Author

*fx.coudert@chimie-paristech.fr

Notes

The authors declare no competing financial interest.

REFERENCES

(1) Furukawa, H.; Cordova, K. E.; O'Keeffe, M.; Yaghi, O. M. *Science* **2013**, *341*, 1230444−1230444.

(2) Hu, A.; Ngo, H. L.; Lin, W. *J. Am. Chem. Soc.* **2003**, *125*, 11490−11491.

(3) Ma, L.; Abney, C.; Lin, W. *Chem. Soc. Rev.* **2009**, *38*, 1248.

(4) Kim, K.; Seo, J. S.; Whang, D.; Lee, H.; Jun, S. I.; Oh, J.; Jeon, Y. J. *Nature* **2000**, *404*, 982−986.

(5) Kepert, C. J.; Prior, T. J.; Rosseinsky, M. J. *J. Am. Chem. Soc.* **2000**, *122*, 5158−5168.

(6) Morris, R. E.; Bu, X. *Nat. Chem.* **2010**, *2*, 353−361.

(7) Zhang, S.-Y.; Li, D.; Guo, D.; Zhang, H.; Shi, W.; Cheng, P.; Wojtas, L.; Zaworotko, M. J. *J. Am. Chem. Soc.* **2015**, *137*, 15406−15409.

(8) Yaghi, O. M.; Li, H.; Eddaoudi, M.; O'Keeffe, M. *Nature* **1999**, *402*, 276−279.

(9) Lin, Z.; Slawin, A. M. Z.; Morris, R. E. *J. Am. Chem. Soc.* **2007**, *129*, 4880−4881.

(10) Zhang, J.; Chen, S.; Nieto, R. A.; Wu, T.; Feng, P.; Bu, X. *Angew. Chem., Int. Ed.* **2010**, *49*, 1267−1270.

(11) Ortiz, A. U.; Boutin, A.; Fuchs, A. H.; Coudert, F.-X. *Phys. Rev. Lett.* **2012**, *109*, 195502.

(12) Ortiz, A. U.; Boutin, A.; Coudert, F.-X. *Chem. Commun.* **2014**, *50*, 5867.

(13) Dovesi, R.; Orlando, R.; Erba, A.; Zicovich-Wilson, C. M.; Civalleri, B.; Casassa, S.; Maschio, L.; Ferrabone, M.; Pierre, M. D. L.; D'Arco, P.; Noël, Y.; Causà, M.; Rérat, M.; Kirtman, B. *Int. J. Quantum Chem.* **2014**, *114*, 1287−1317.

(14) Peintinger, M. F.; Oliveira, D. V.; Bredow, T. *J. Comput. Chem.* **2013**, *34*, 451−459.

(15) Perdew, J. P.; Ruzsinszky, A.; Csonka, G. I.; Vydrov, O. A.; Scuseria, G. E.; Constantin, L. A.; Zhou, X.; Burke, K. *Phys. Rev. Lett.* **2008**, *100*, 136406.

(16) Adamo, C.; Barone, V. *J. Chem. Phys.* **1999**, *110*, 6158.

(17) Brozek, C. K.; Michaelis, V. K.; Ong, T.-C.; Bellarosa, L.; López, N.; Griffin, R. G.; Dincă, M. *ACS Cent. Sci.* **2015**, *1*, 252−260.

(18) Grimme, S. *J. Comput. Chem.* **2006**, *27*, 1787−1799.

(19) Dubbeldam, D.; Calero, S.; Ellis, D. E.; Snurr, R. Q. *Mol. Simul.* **2016**, *42*, 81−101.

(20) Amirjalayer, S.; Tafipolsky, M.; Schmid, R. *Angew. Chem., Int. Ed.* **2007**, *46*, 463−466.

(21) Amirjalayer, S.; Schmid, R. *Microporous Mesoporous Mater.* **2009**, *125*, 90−96.

(22) Birch, F. *Phys. Rev.* **1947**, *71*, 809−824.

(23) Graham, A. J.; Allan, D. R.; Muszkiewicz, A.; Morrison, C. A.; Moggach, S. A. *Angew. Chem., Int. Ed.* **2011**, *50*, 11138−11141.

(24) Chapman, K. W.; Halder, G. J.; Chupas, P. J. *J. Am. Chem. Soc.* **2009**, *131*, 17546−17547.

(25) Ma, Q.; Yang, Q.; Ghoufi, A.; Férey, G.; Zhong, C.; Maurin, G. *Dalton Trans.* **2012**, *41*, 3915−3919.

(26) Greathouse, J. A.; Allendorf, M. D. *J. Am. Chem. Soc.* **2006**, *128*, 10678−10679.

(27) Zhou, W.; Wu, H.; Yildirim, T.; Simpson, J. R.; Walker, A. R. H. *Phys. Rev. B: Condens. Matter Mater. Phys.* **2008**, *78*, 054114.

(28) Coudert, F.-X.; Fuchs, A. H.; Neimark, A. V. *Phys. Chem. Chem. Phys.* **2014**, *16*, 4394.

(29) Joo, J.; Kim, H.; Han, S. S. *Phys. Chem. Chem. Phys.* **2013**, *15*, 18822.

(30) Liu, M.; Little, M. A.; Jelfs, K. E.; Jones, J. T. A.; Schmidtmann, M.; Chong, S. Y.; Hasell, T.; Cooper, A. I. *J. Am. Chem. Soc.* **2014**, *136*, 7583−7586.